Supplementary information: Disorder-induced coherent pulses in direct-current driven external-cavity laser arrays

Greggory Scranton[1], Kendall Golden[2], Olivier Spitz[1,*], Arindam Mishra[1], Igor Belykh[2,†], and Yehuda Braiman[1,3,‡]

[1]The College of Optics and Photonics (CREOL), University of Central Florida, Orlando, FL 32816, USA
[2]Department of Mathematics and Statistics and Neuroscience Institute, Georgia State University, P.O. Box 4110, Atlanta, Georgia, 30302-410, USA
[3]Department of Electrical and Computer Engineering, University of Central Florida, Orlando, FL 32816, USA
[*]olivier.spitz@ucf.edu
[†]ibelykh@gsu.edu
[‡]yehuda.braiman@ucf.edu

Single-laser dynamics with the Lang-Kobayashi models

The peculiarity of pulsing within the framework of this study is that it requires a network of emitters to be triggered. This process can be optimized with adequate disordered frequency detuning, as highlighted in the main text. Yet, our model can also be studied in the context of a single laser subject to external optical feedback, and in this case, it does not show pulsing dynamics. Details about the nonlinear dynamics that can be observed in this configuration are found in Fig. 1, and those states are in good agreement with prior studies about the same configuration.[1,2] It is relevant to note that, in the case of an array of lasers, the same dynamics can also be observed, but we only focused on the pulsing state as it has not been reported previously. For a high bias current (seven times) above the threshold, Fig. 1 (a) shows that the single laser exhibits a steady-state behavior up to an intermediate feedback level of 10 ns^{-1}. The corresponding unwrapped phase in Fig. 1 (b) is monotonically decreasing and no specific feature is highlighted in the electrical spectrum of Fig. 1 (c). Further increase of the feedback strength to 10.7 ns^{-1} triggers a first kind of switching dynamics in the output of the laser, as one can observe in Fig. 1 (d). Switching dynamics correspond to a train of pulses, as opposed to the pulsing dynamics shown in the main text for arrays of lasers. Each train of pulses is composed of many pulses, and the overall behavior is periodic. As mentioned, we found no single pulsing configuration for the lone laser under external optical feedback. The typical phase behavior of switching dynamics, shown in Fig. 1 (e), is also very different from the phase behavior during pulsing, which will be discussed in an upcoming figure. Phase increases in steps during the pulse train and then abruptly decreases outside the pulse train, with a diminution over several periods. The electrical spectrum in Fig. 1 (f) comprises several broad components of discrete peaks. The interval between these multiple peaks corresponds to the repetition frequency of the switching dynamics. The oscillation frequency within the switching dynamics corresponds to the maximum of the electrical spectrum. From this feedback strength value, a slight increase tunes the switching dynamics, as visualized in Fig. 1 (g). The laser output still displays a train of pulses, but the number of pulses within the train has increased, and the amplitude of the pulses is more consistent. The evolution of phase in Fig. 1 (h) underscores that the two switching dynamics share similar features, and that confirms the difference with pulsing dynamics. The electrical spectrum shown in Fig. 1 (i) does not differ much from that shown in Fig. 1 (f), but each peak is broadened. A wide variety of switching dynamics (not shown here) can be obtained when varying κ^f around 11-14 ns^{-1}. When the feedback strength is increased, the train of pulses contains more and more pulses until it becomes continuous, and only the fast oscillation remains. Such state can be observed in Fig. 1 (j) for $\kappa^f = 17$ ns^{-1}. The phase decreases over long time scales and otherwise follows the oscillation pattern at short time scales, as seen in Fig. 1 (k). The electrical spectrum in Fig. 1 (l) contains the frequency component related to the oscillation frequency and several harmonics of the main frequency. Each contribution is narrow-band, contrasting with the electrical spectra for switching dynamics. In this single-laser configuration, intermediate feedback strength can also lead to low-complexity chaos dynamics, and this is illustrated in Fig. 1 (m) for $\kappa^f = 25$ ns^{-1}. The phase in Fig. 1 (n) now decreases much faster with time and shows small amplitude fluctuations that seem to retain an almost periodic behavior with a typical scale close to roundtrip time (3 ns). The electrical spectrum in Fig. 1 (o) displays a wide component, which is a typical feature of chaos dynamics, but discrete peaks can still be found within the structure, hence explaining why the temporal pattern of Fig. 1 (m) belongs to low-complexity chaos.

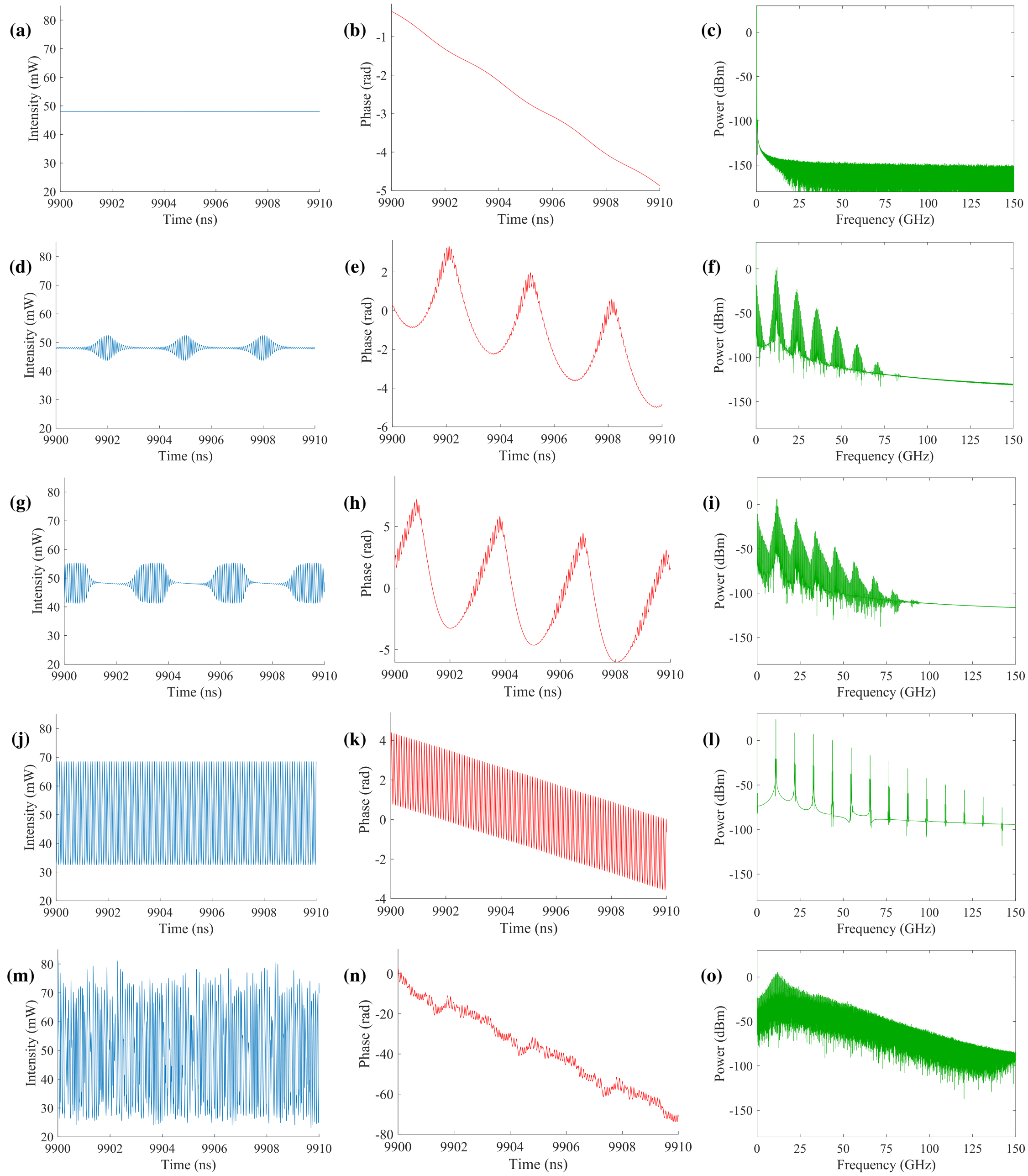

Supplementary figure 1. Nonlinear dynamics that can be observed for a bias current high above threshold ($\beta = 7$) and several conditions of feedback strength in a single laser; (a) Intensity time trace, (b) phase time trace, and (c) electrical spectrum for $\kappa^f = 10$ ns^{-1}, illustrating steady-state dynamics at low feedback strength; (d-f) identical to (a-c) but for $\kappa^f = 10.7$ ns^{-1}, corresponding to a first type of switching dynamics; (g-i) identical to (a-c) but for $\kappa^f = 11$ ns^{-1}, corresponding to a second type of switching dynamics; (j-l) identical to (a-c) but for $\kappa^f = 17$ ns^{-1}, corresponding to fast oscillations in the output of the laser; (m-o) identical to (a-c) but for $\kappa^f = 25$ ns^{-1}, corresponding to low-complexity chaos dynamics. The frequency detuning for this laser is 0. Other parameters not mentioned here are as shown in Tab. 1

Default parameters for the Lang-Kobayashi model simulations

The Lang-Kobayashi model in the context of an array of semiconductor lasers takes into account various dynamical parameters that we list in this section, and the values for each parameter used in the 30 laser models of the main text are gathered in Table 1. The relationship between the threshold current J_{th}, defined as a number of electrons per unit of time (used in the equations) and I_{th}, the threshold current in unit of A (described in the table) is $J_{th} = \frac{I_{th}}{e}$, with e the charge of an electron. An illustration of decay non-local coupling is shown in Fig. 2. The external time delay is identical for all lasers in all the simulations presented. Yet, similarly to what has already been mentioned for noise, we have computationally verified the emergence of pulses in the presence of disordered time delay but wished to restrain to non-disordered examples to explain the pulsing mechanism better and compare with reduced modeling. Tab. 3 shows the parameters used in the two-laser Lang-Kobayashi model, whose simulation results are shown in Fig. 4(a) in the main text.

Supplementary table 1. Details of the parameters for simulating the 30-Lang-Kobayashi laser model array. The values used in the simulations are compatible with those usually found in semiconductor lasers.[3,4]

Symbol	Description	Value
λ	Wavelength	770 nm
α	Linewidth enhancement factor	5.0
g	Differential gain coefficient	1.5×10^{-5} ns^{-1}
s	Gain saturation coefficient	2×10^{-7}
γ	Cavity loss	500 ns^{-1}
N_0	Carrier number at transparency	1.5×10^{8}
γ_{n}	Carrier loss rate	0.5 ns^{-1}
ω_{odd}	Frequency detuning for odd lasers	-2 GHz
ω_{even}	Frequency detuning for even lasers	2 GHz
τ	Feedback delay time	3 ns
κ^{f}	Feedback strength	varied from 0 ns^{-1}to 50 ns^{-1}in steps of 0.2 ns^{-1}
d	Cross-laser reinjection efficiency	0.75
β	Pump factor	varied up to 9.0
I_{th}	Threshold pump current for a single laser	14.7 mA

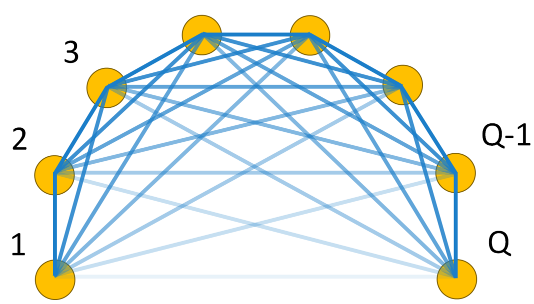

Supplementary figure 2. Decay non-local coupling in the network of emitters. The transparency of the links is inversely proportional to the coupling strength between emitters.

Perturbation of the frequency detuning in the 30-laser configuration

The main manuscript details the pulsing dynamics in an array of 30 lasers with frequency detuning. To optimize the pulsing dynamics, which includes the juxtaposition of anti-phase and in-phase synchrony, we focused on a configuration with a frequency detuning of -2 GHz for odd lasers and 2 GHz for even lasers. However, this requirement can be relaxed without significantly impacting the observed dynamics. With the frequency detuning values listed in Tab. 2, one can observe the pulsing dynamics displayed in Fig. 3, among others. A configuration with a single pulse per period is illustrated in Fig. 3 (a) for the full array of 30 lasers, and the alternate behavior between the even and the odd lasers is still observed. In Fig. 3 (b) the phase time trace for an even and an odd laser shows that the phase behavior strongly differs compared to what was described in Fig. 1 for a single laser. The phase is overall decreasing and there is a positive step every time a pulse is triggered for the even lasers while there is a negative step every time a pulse is triggered for the odd lasers. The synchrony behavior is detailed in Fig. 3 (c) and shows again that anti-phase synchrony is followed by in-phase synchrony. Pulsing in the odd lasers is simultaneous with the anti-phase behavior, while pulsing in the even lasers is simultaneous with the in-phase behavior. We also highlight a case with two pulses per period, as seen in Fig. 3 (d). The phase time trace in Fig. 3 (e) confirms that the number of steps is related to the

Supplementary table 2. Frequency detuning of the 30 lasers in the array when the perturbed case is studied.

Laser number	Frequency detuning (GHz)
1	-2.059
2	2.008
3	-2.079
4	1.887
5	-1.998
6	2.117
7	-2.041
8	2.035
9	-1.930
10	2.008
11	-1.952
12	2.155
13	-1.781
14	2.020
15	-2.178
16	2.033
17	-1.982
18	1.893
19	-1.998
20	2.032
21	-1.883
22	2.011
23	-2.108
24	2.128
25	-2.016
26	2.068
27	-1.978
28	2.072
29	-2.028
30	2.017

number of pulses, as two steps per period can be observed. The last panel, meaning Fig. 3 (f), showcases the synchrony features already observed without the perturbation of the frequency detuning. Overall, this example underscores that the frequency detuning does not need to be strictly -2 or 2 GHz to observe pulsing and an uncertainty of more than 0.1 GHz can be tolerated for some lasers in the array. This finding is noteworthy as it can be complex to experimentally manufacture an array of lasers with extremely precise frequency detuning. A typical uncertainty of 0.1 GHz can be achieved more realistically and should not impact the pulsing phenomenon. This alternating configuration of detuning values was engineered to encourage pulsing, but pulsing can be achieved with other non-alternating configurations, as demonstrated in the next section.

Example with sparse frequency detuning configuration

In addition to the perturbed frequency detuning that is underscored in the previous section, pulsing was achieved in an example with a non-alternating detuning configuration. This example has an array of 20 lasers, and its behavior is illustrated in Fig. 4. The frequency detuning on lasers 5, 10, and 15 is 4 GHz. All other lasers have a detuning of zero. Other parameters are the same as those shown in Tab. 1. Pulsing has the greatest amplitude on the three lasers with 4 GHz detuning. The amplitude of the pulses is weaker for lasers farther from these detuned lasers, with the lasers on the edges showing the lowest amplitude pulses. This further proves that pulsing is driven by differences in frequency detuning between lasers in an array. The synchrony behavior shows anti-phase synchrony followed by in-phase synchrony, as seen in Fig. 4(c) and (f), although neither is as pronounced as in the alternating-detuning cases.

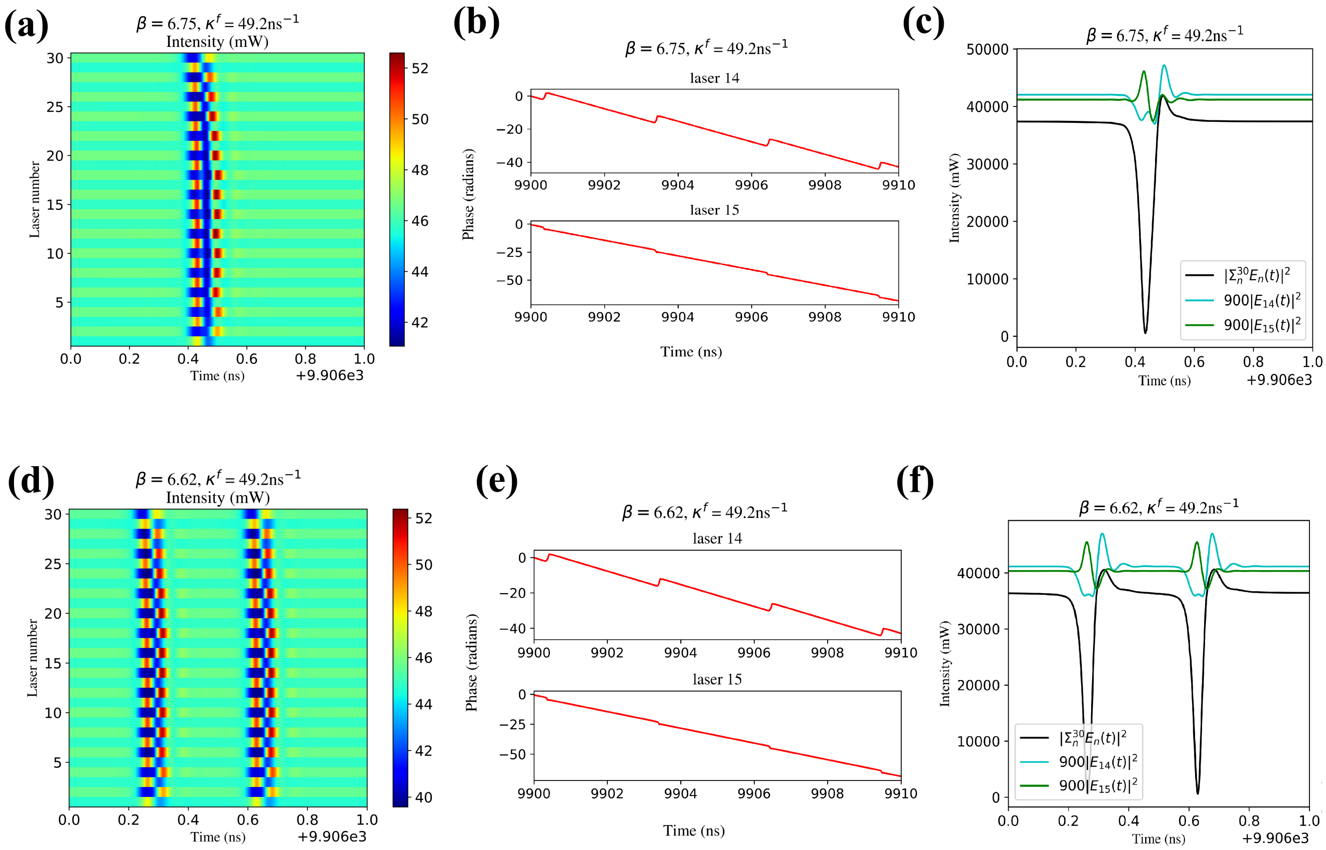

Supplementary figure 3. Investigation of a 30-laser pulsing case similar to the one highlighted in the main text, but with the addition of perturbed frequency detuning. (a) Overview of single pulsing in the array of 30 lasers, with the odd and even lasers showing alternate behaviors. (b) Phase time trace for one selected odd laser and one selected even laser, both showing a step at the instant of pulsing that contrasts with the otherwise linear evolution of the phase. (c) Combined field intensity (black curve) of the 30 lasers in the array, illustrating when the lasers are anti-phase synchronized and in-phase synchronized. This panel also shows the magnified intensity of an odd laser (green curve) and an even laser (cyan curve). (c-d) identical to (a-b) but for a configuration with two pulses per period.

Computation support for deriving the reduced model

The objective of the reduced model is to explain the origin of the pulsing behavior in the minimum network required to generate pulsing, which is a network of two lasers with transverse coupling. The parameters used in the two-laser model shown in Fig. 4(a) of the main text are summarized in Tab. 3. To derive the reduced model, we approximate $r_1(t-\tau) \approx r_1(t) \approx r_2(t-\tau) \approx r_2(t)$, $\phi_i(t-\tau) \approx \phi_i(t)$, and $N_1(t-\tau) \approx N_1(t) \approx N_2(t-\tau) \approx N_2(t)$. To demonstrate the validity of these approximations for the two-laser case, example plots are shown in Fig. 5 for the pulsing case in which $\kappa^f = 18.0ns^{-1}$ and $\Delta\omega = 3.0GHz$.

The normalized differences between the non-delayed and time-delayed versions of $r_2(t)$, $\phi_2(t)$, and $N_2(t)$ are plotted in Fig. 5(a). The absolute value of $(\phi_2(t) - \phi_2(t-\tau))/\phi_2(t)$ is below 5×10^{-5} for all time, and remains below 1.2×10^{-5} between pulses. The absolute value of $(N_2(t) - N_2(t-\tau))/N_2(t)$ is below 0.02 for all time and remains below 2×10^{-6} between pulses. The absolute value of $(r_2(t) - r_2(t-\tau))/r_2(t)$ is slightly larger, at a maximum around 0.2, but remains below 1×10^{-5} between pulses. This maximum value may be due to a period that differs slightly from τ or small differences in pulse shapes. The fact that all these values remain around zero for most of the time supports the approximations $r_2(t-\tau) \approx r_2(t)$, $\phi_2(t-\tau) \approx \phi_2(t)$, and $N_2(t-\tau) \approx N_2(t)$. The same trends hold true for laser 1, so $r_1(t-\tau) \approx r_1(t)$, $\phi_1(t-\tau) \approx \phi_1(t)$, and $N_1(t-\tau) \approx N_1(t)$.

The normalized differences between the $r_i(t)$ and $N_i(t)$ values for the two lasers are shown in Fig. 5(b). The absolute value of $(N_2(t) - N_1(t))/N_2(t)$ is below 0.025 for all time, and remains below 4.1×10^{-3} between pulses. The absolute value of $(r_2(t) - r_1(t))/r_2(t)$ is slightly larger, at a maximum under 0.2, but remains below 0.013 between pulses. As before, the fact these values are generally around zero validates the approximation $r_1(t) \approx r_2(t)$ and $N_1(t) \approx N_2(t)$.

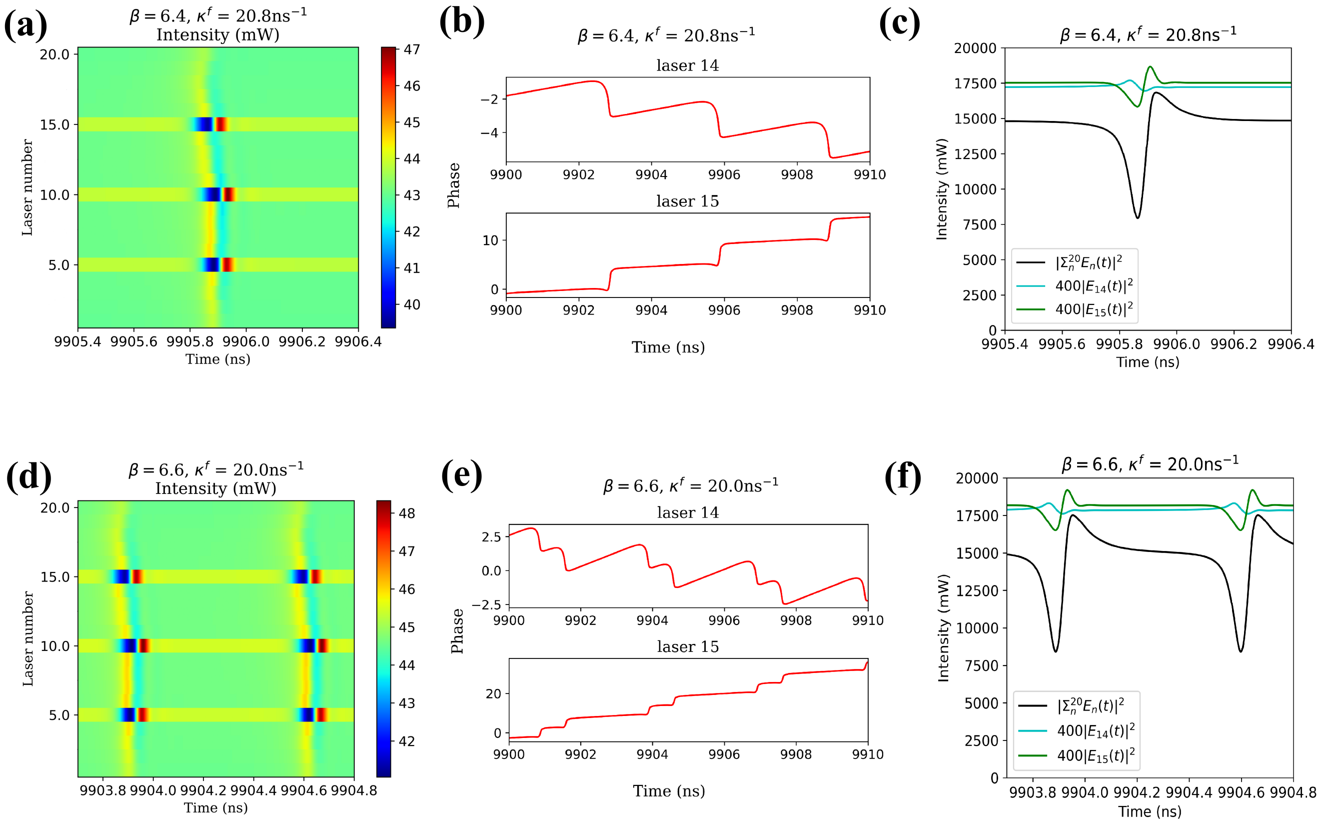

Supplementary figure 4. Investigation of a 20-laser pulsing case when a limited number of emitters in the array exhibit frequency detuning, with only $\omega_5 = \omega_{10} = \omega_{15} = 4$ GHz being non-zero. (a) Overview of single pulsing in the array of 20 lasers. (b) Phase time trace for one selected odd laser and one selected even laser, both showing a step at the instant of pulsing that contrasts with the otherwise linear evolution of the phase. (c) Combined field intensity (black curve) of the 20 lasers in the array, illustrating when the lasers are anti-phase synchronized and in-phase synchronized. This panel also shows the magnified intensity of an odd laser (green curve) and the magnified intensity of an even laser (cyan curve). (c-d) identical to (a-b) but for a configuration with two pulses per period.

Supplementary table 3. Details of the parameters for simulating the two-Lang-Kobayashi laser model array.

Symbol	Description	Value
λ	Wavelength	770 nm
α	Linewidth enhancement factor	2.5
g	Differential gain coefficient	1.5×10^{-5} ns^{-1}
s	Gain saturation coefficient	2×10^{-7}
γ	Cavity loss	500 ns^{-1}
N_0	Carrier number at transparency	1.5×10^{8}
γ_n	Carrier loss rate	0.5 ns^{-1}
ω_1	Frequency detuning for laser 1	-$\Delta\omega/2$
ω_2	Frequency detuning for laser 2	$\Delta\omega/2$
τ	Feedback delay time	8 ns
κ^f	Feedback strength	varied from 6 ns^{-1}to 24 ns^{-1}in steps of 0.2 ns^{-1}
d	Cross-laser reinjection efficiency	1.0
β	Pump factor	9.0
I_{th}	Threshold pump current for a single laser	14.7 mA

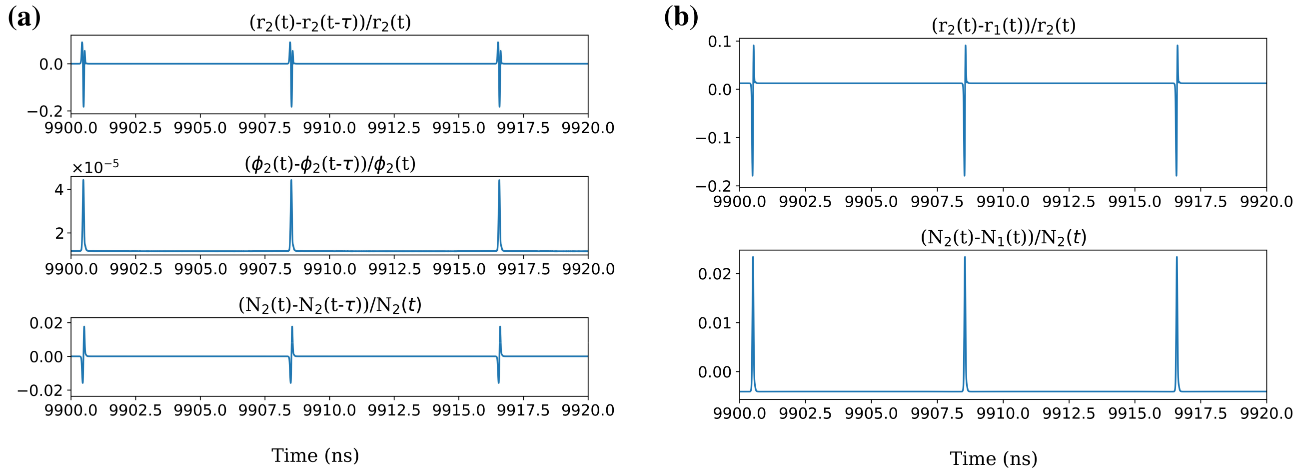

Supplementary figure 5. Plots demonstrating the validity of the approximations used for the reduced model. These are shown for the two laser full Lang-Kobayashi model simulations for the pulsing case in which $\kappa^f = 18.0ns^{-1}$ and $\Delta\omega = 3.0GHz$. (a) normalized differences between non-delayed and time-delayed versions of $r_2(t)$, $\phi_2(t)$, and $N_2(t)$. (b) normalized differences between the $r_i(t)$ and $N_i(t)$ values for the different lasers.

Supplementary References

1. Masoller, C. Spatiotemporal dynamics in the coherence collapsed regime of semiconductor lasers with optical feedback. Chaos: An Interdisciplinary Journal of Nonlinear Science 7, 455–462 (1997).

2. Dong, J.-X. Ruan, J. Zhang, L. Zhuang, J.-P. & Chan, S.-C. Stable-unstable switching dynamics in semiconductor lasers with external cavities. Physical Review A 103, 053524 (2021).

3. Liu, B. Braiman, Y. Nair, N. Lu, Y. Guo, Y. Colet, P. & Wardlaw, M. Nonlinear dynamics and synchronization of an array of single mode laser diodes in external cavity subject to current modulation. Optics Communications 324, 301–310 (2014).

4. Nair, N. Hu, K. Berrill, M. Wiesenfeld, K. & Braiman, Y. Using disorder to overcome disorder: A mechanism for frequency and phase synchronization of diode laser arrays. Physical Review Letters 127, 173901 (2021).